Acta Crystallographica Section F
Structural Biology and Crystallization Communications
ISSN 1744-3091

Structure of *N*-formylglycinamide ribonucleotide amidotransferase II (PurL) from *Thermus thermophilus* HB8

Sakiko Suzuki,[a] Hisaaki Yanai,[b] Mayumi Kanagawa,[b] Satoko Tamura,[a] Yuzo Watanabe,[a] Kyotaro Fuse,[a] Seiki Baba,[b] Gen-ichi Sampei[b,c] and Gota Kawai[a,b]*

[a]Department of Life and Environmental Sciences, Faculty of Engineering, Chiba Institute of Technology, Narashino, Chiba 275-0016, Japan, [b]RIKEN SPring-8 Center, Harima Institute, 1-1-1 Kouto, Sayo, Hyogo 679-5148, Japan, and [c]Department of Engineering Science, Graduate School of Informatics and Engineering, The University of Electro-Communications, 1-5-1 Chofugaoka, Chofu, Tokyo 182-8585, Japan

Correspondence e-mail: gkawai@sea.it-chiba.ac.jp

Received 29 July 2011
Accepted 14 November 2011

PDB Reference: PurL, 3viu.

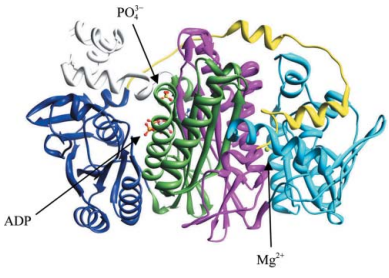

The crystal structure of PurL from *Thermus thermophilus* HB8 (*Tt*PurL; TTHA1519) was determined in complex with an adenine nucleotide, PO_4^{3-} and Mg^{2+} at 2.35 Å resolution. *Tt*PurL consists of 29 α-helices and 28 β-strands, and one loop is disordered. *Tt*PurL consists of four domains, A1, A2, B1 and B2, and the structures of the A1–B1 and A2–B2 domains were almost identical to each other. Although the sequence identity between *Tt*PurL and PurL from *Thermotoga maritima* (*Tm*PurL) is higher than that between *Tt*PurL and the PurL domain of the large PurL from *Salmonella typhimurium* (*St*PurL), the secondary structure of *Tt*PurL is much more similar to that of *St*PurL than to that of *Tm*PurL.

1. Introduction

The fourth reaction of the purine nucleotide biosynthetic pathway is an ATP-dependent amide transfer in which *N*-formylglycinamide ribonucleotide (FGAR), glutamine and ATP are converted to *N*-formylglycinamidine ribonucleotide (FGAM), glutamate and ADP (Melnick & Buchanan, 1957). In Gram-positive bacteria and archaea, the enzyme that catalyzes this reaction, FGAR amidotransferase, is composed of three subunits (Ebbole & Zalkin, 1987; Saxild & Nygaard, 2000; Zhang *et al.*, 2008). FGAR amidotransferase I, also called PurQ, produces an ammonia molecule by converting glutamine to glutamate. FGAR amidotransferase II, also called PurL, transfers the ammonia molecule to FGAR to form FGAM in an ATP-dependent manner. The third subunit is called FGAR amidotransferase III or PurS; it interacts with PurQ and PurL and is thought to assist in the transfer of the ammonia molecule from PurQ to PurL (Hoskins *et al.*, 2004). Interestingly, in Gram-negative bacteria and eukaryotes the enzyme is a single polypeptide with three domains, which correspond to the three subunits of the counterpart, and is called large PurL. The crystal structures of the complex of *Thermotoga maritima* PurQ, PurL and PurS and of *Salmonella typhimurium* large PurL have been determined and it was found that the overall structures of the complex and large PurL are similar to each other (Anand, Hoskins, Stubbe *et al.*, 2004; Morar *et al.*, 2008). The structure of *T. maritima* PurL has also been determined in the free form as well as in complexes with ADP, AMPPCP, ATP or FGAR (Morar *et al.*, 2006; Mathews *et al.*, 2006). However, the reaction mechanism, including the transfer of the ammonia molecule, is not yet well known. To elucidate the reaction mechanism of *N*-formylglycinamide ribonucleotide amidotransferase, including the molecular interactions among the three subunits as well as the movement of the ammonia molecule, we are conducting a structural analysis of PurL, PurQ and PurS from *Thermus thermophilus* HB8. In the present study, the crystal structure of *T. thermophilus* PurL was determined in complex with an adenine nucleotide at 2.35 Å resolution.

2. Materials and methods

2.1. Protein expression and purification

The TTHA1519 gene was amplified by PCR using *T. thermophilus* HB8 genomic DNA as the template. The amplified fragment was cloned under the control of the T7 promoter of the *Escherichia coli*

expression vector pET-11a (Novagen, Madison, Wisconsin, USA). The expression vector was introduced into *E. coli* Rosetta 834 (DE3) strain and the recombinant strain was cultured in 12 l LB medium supplemented with 50 mg ml^{-1} ampicillin in the presence of selenomethionine. The collected cells (33.5 g) were suspended in 20 m*M*

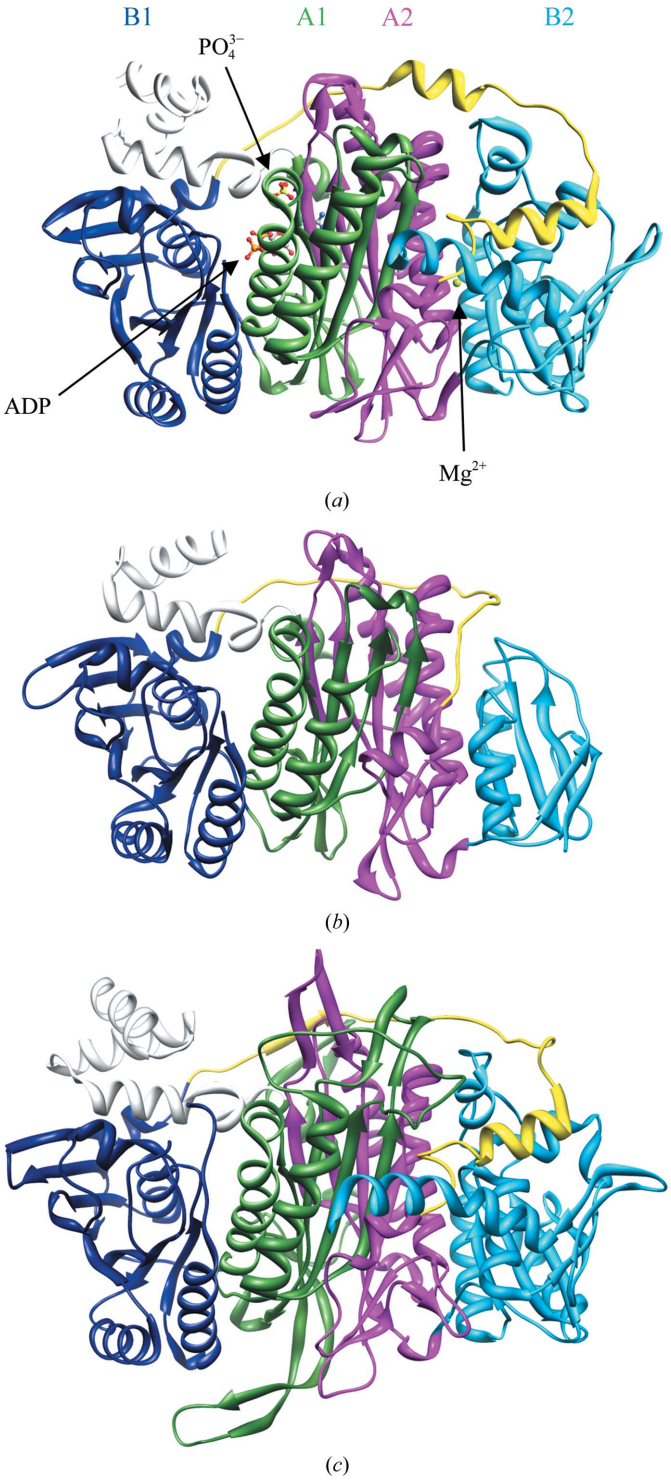

Figure 1
Overall structures of PurLs. The A1, B1, A2 and B2 domains are indicated in green, blue, magenta and cyan, respectively. The N-terminal flanking sequence and the linker between the B1 and A2 domains are indicated in grey and yellow, respectively. (*a*) *Tt*PurL, (*b*) *Tm*PurL (PDB entry 2hru), (*c*) *St*PurL (PDB entry 1t3t). The locations of bound ADP, PO_4^{3-} and Mg^{2+} are also shown in (*a*).

Table 1
Data-collection and refinement statistics.

Values in parentheses are for the highest resolution shell.

Data set	Peak	Edge	Remote
Space group	$C222_1$	$C222_1$	$C222_1$
Unit-cell parameters (Å)			
a	94.9	94.8	94.9
b	94.6	94.7	94.6
c	158.8	159.2	158.9
Diffraction data			
Wavelength (Å)	0.9793	0.9795	1.0000
Resolution (Å)	2.35 (2.43–2.35)	2.70 (2.80–2.70)	2.70 (2.80–2.70)
Measured reflections	180802	135770	133393
No. of unique reflections	29532	20028	19946
Completeness (%)	97.3 (78.2)	100.0 (100.0)	100.0 (99.9)
R_{merge}† (%)	12.0 (36.8)	11.0 (29.5)	11.1 (28.1)
$\langle I/\sigma(I)\rangle$	14.0 (2.1)	11.4 (4.9)	11.8 (5.5)
Refinement			
Resolution limits (Å)	47.28–2.35 (2.50–2.35)		
R factor (%)	19.9 (25.4)		
R_{free} (%)	26.2 (29.7)		
Test-set size for R_{free} (%)	10.0		
No. of atoms			
Protein	5371		
Ligand	40		
Water	296		
R.m.s. deviations			
Bond lengths (Å)	0.006		
Bond angles (°)	1.30		
Mean *B* factors (Å^2)			
Main-chain atoms	23.37		
Side-chain atoms	26.55		
Ligand atoms	45.20		
Water atoms	31.34		
Ramachandran plot			
Favoured region	674		
Allowed region	23		
Outlier region	2		

† $R_{merge} = \sum_{hkl}\sum_i |I_i(hkl) - \langle I(hkl)\rangle| / \sum_{hkl}\sum_i I_i(hkl)$, where $I_i(hkl)$ is the observed intensity and $\langle I(hkl)\rangle$ is the average intensity for multiple measurements.

Tris–HCl buffer pH 8.0 containing 50 m*M* NaCl and then disrupted by sonication. The cell lysate was incubated at 343 K for 10 min and kept on ice. The soluble fraction after ultracentrifugation at 200 000*g* and 277 K was applied onto a Resource ISO column (GE Healthcare, UK) equilibrated with 50 m*M* sodium phosphate buffer pH 7.0 containing 1.5 *M* ammonium sulfate and eluted with a linear gradient of 1.5–0 *M* ammonium sulfate. The *Tt*PurL fractions were applied onto a Resource Q column (GE Healthcare, UK) equilibrated with 20 m*M* Tris–HCl pH 8.0, which was eluted with a linear gradient of 0–0.5 *M* NaCl. The fractions containing *Tt*PurL were applied onto a hydroxyapatite CHT10-I column (Bio-Rad, USA) equilibrated with 0.01 *M* sodium phosphate buffer pH 7.0 containing 150 m*M* NaCl, which was eluted with a linear gradient of 0.01–0.5 *M* sodium phosphate buffer containing 150 m*M* NaCl. The collected *Tt*PurL fractions were applied onto a HiLoad 16/60 Superdex 75 column (GE Healthcare, UK) equilibrated with 20 m*M* Tris–HCl pH 8.0 containing 150 m*M* NaCl. The protein solution was desalted on a HiPrep 26/10 desalting column (GE Healthcare, UK) and concentrated to 22.9 mg ml^{-1}. The protein concentration was estimated from the UV absorption at 280 nm. The overall yield was estimated to be 5.3 mg from 12 l culture.

2.2. Crystallization, data collection and structure determination

*Tt*PurL was crystallized by the hanging-drop vapour-diffusion method. 1 µl protein solution (7.63 mg ml^{-1} in 20 m*M* Tris–HCl pH 8.0, 1 m*M* DTT) was mixed with an equal volume of reservoir solution consisting of 25% PEG 3350, 0.2 *M* ammonium acetate and 0.1 *M* MES buffer pH 7.1, and 1 µl 1 m*M* AMPPNP was added. The

mixed solution was then equilibrated against 100 µl reservoir solution at 293 K.

Diffraction data sets were collected at 100 K using wavelengths of 0.9793, 0.9795 and 1.0000 Å for peak, edge and remote data sets, respectively, on the RIKEN Structural Genomics Beamline I (BL26B1; Ueno *et al.*, 2006) at SPring-8 (Hyogo, Japan). The data were processed using the *HKL*-2000 program package (Otwinowski & Minor, 1997; Table 1). The space group of the obtained crystal was $C222_1$ and the unit-cell parameters were $a = 94.9$, $b = 94.6$, $c = 158.8$ Å. There is one monomer in the asymmetric unit and 45.2% of the crystal volume is occupied by solvent.

The structure of *Tt*PurL was solved by the MAD method using *SOLVE*/*RESOLVE* (Terwilliger & Berendzen, 1999; Terwilliger, 2000, 2003). The program *CNS* (Brünger *et al.*, 1998) was used for cycles of refinement. After each round of refinement, the model was refitted to the OMIT electron-density map using the program *O* (Jones *et al.*, 1991). Water molecules were picked up from difference maps on the basis of peak height and distance criteria (Morris *et al.*,

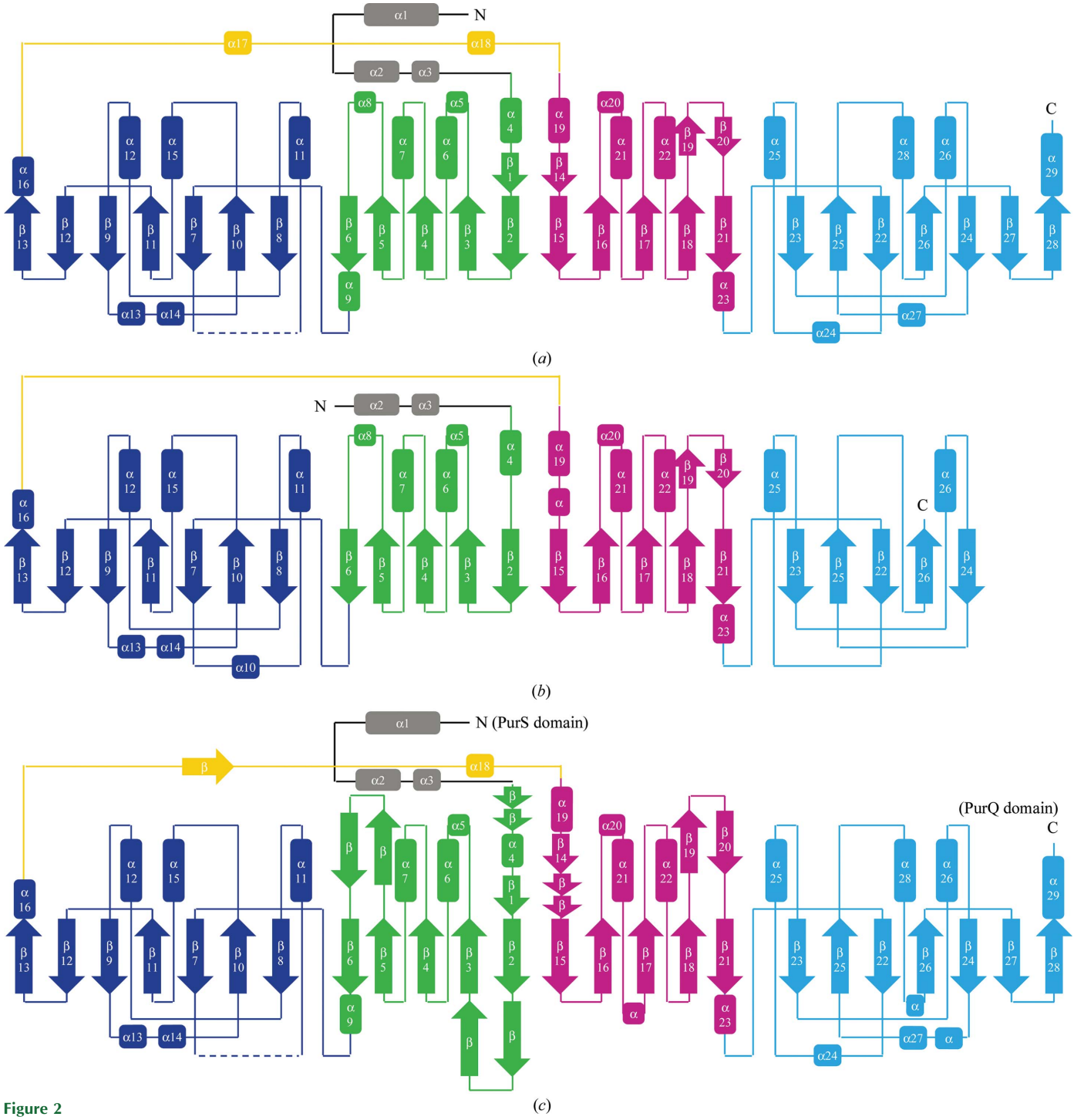

Figure 2
Secondary structures of PurLs. The same colour scheme is used as in Fig. 1. (*a*) *Tt*PurL, (*b*) *Tm*PurL, (*c*) *St*PurL. The existence of α10 in *Tm*PurL was confirmed by the structures 2hs3 and 2hs4.

2002). The quality of the models was validated with *PROCHECK* (Laskowski *et al.*, 1993). Refinement statistics are shown in Table 1. Structure diagrams were produced using the program *Chimera* (Pettersen *et al.*, 2004).

The atomic coordinates and structure factors have been deposited in the PDB as entry 3viu.

3. Results and discussion

3.1. Overall structure

The overall structure of *Tt*PurL, which consists of four domains, is shown in Figs. 1(*a*) and 2(*a*). *Tt*PurL consists of 29 α-helices and 28 β-strands, including a missing α-helix which is expected to exist between β7 and α11 in the disordered loop, 210–231, in the B1 domain (Fig. 2). The existence of the missing α-helix is supported by comparison with the known PurL structures as well as the fact that the corresponding region in the B2 domain forms helix α24. *Tt*PurL has an approximate twofold axis.

As shown in Fig. 3, the structures of the A1–B1 and the A2–B2 domains are almost identical to each other, indicating that this protein is generated by a gene duplication (Anand, Hoskins, Bennett *et al.*, 2004; Anand, Hoskins, Stubbe *et al.*, 2004). It should be noted that the sequence identity and similarity between the A1–B1 and the A2–B2 domains are only 21% and 31%, respectively, even when an improved method for amino-acid sequence alignment by introducing solvent accessibility, *ALAdeGAP* (Hijikata *et al.*, 2011), is used. Small differences in the structures of the A1–B1 and A2–B2 domains can be found; the small helix α8 in the A1 domain is replaced by β19 and β20 in the A2 domain and the small helix α13 in the B1 domain is replaced by a short loop in the B2 domain. Helix α3 in the N-terminal flanking sequence and helix α18 in the linker sequence between the B1 and A2 domains are located in corresponding positions, suggesting that the N-terminal flanking sequence and the linker sequence are also generated by the gene duplication.

The phosphoribosylaminoimidazole synthetase PurM consists of two domains, A and B, and the structure of the monomer is similar to the A1–B1 or A2–B2 domains of PurL (Li *et al.*, 1999). The relative positions of the A1–B1 and A2–B2 domains are also similar to those of the two subunits of PurM, suggesting that the PurL gene was generated from the PurM gene: the ancestral PurL gene was generated by gene duplication of PurM. PurM catalyzes the next reaction to PurL and both of these enzymes catalyze reactions in which a carbonyl group is activated by ATP and a C—N bond is then formed.

3.2. Structural comparison

In general, the overall structure of *Tt*PurL is similar to those of *Tm*PurL and *St*PurL, as shown in Figs. 1(*b*), 1(*c*), 2(*b*) and 2(*c*). The structures of the A1, B1 and A2 domains are similar to those of *Tm*PurL and the location of the adenine nucleotide is also similar in the two PurLs. However, the structures of the B2 domains of these proteins are significantly different from each other. The divergence in the B2 domains is probably responsible for the loss of catalytic activity in the B2 domain as well as the interaction with PurS or PurQ (Anand, Hoskins, Bennett *et al.*, 2004; Morar *et al.*, 2008). It is noted that most of the secondary-structural elements found in *Tt*PurL are also found in *St*PurL, although *St*PurL has some insertions of α-helices and β-sheets (Fig. 2). The sequence identity analyzed by *ALAdeGAP* (Hijikata *et al.*, 2011) between *Tt*PurL and *Tm*PurL is 34% and that between *Tt*PurL and *St*PurL is 20%. In contrast, for the B2 domains the sequence identity between *Tt*PurL and *Tm*PurL is 12% and that between *Tt*PurL and *St*PurL is 22%. This also shows the structural divergence in the B2 domain of *Tm*PurL and the structural similarity throughout the four domains between *Tt*PurL and *Tm*PurL.

The conformation of the linker sequence between the B1 and A1 domains of *Tt*PurL is similar to that in *St*PurL, except for α17, as shown in Figs. 1 and 2 (shown in yellow). The linker sequence of *Tm*PurL is shorter than those of *Tt*PurL and *St*PurL and the conformation is also different. The conformations of the N-terminal flanking sequences are similar in the three PurLs, although *Tm*PurL lacks α1.

3.3. Ligand binding

Three ligands, adenine nucleotide, PO_4^{3-} and Mg^{2+}, were found in the crystal structure of PurL (Fig. 1*a*), and the OMIT map for the adenine nucleotide and PO_4^{3-} is also shown in Fig. 4(*a*). An adenine nucleotide binds to the B1-domain side of the A1 and A2 domains, which is thought to be the active site (Anand, Hoskins, Stubbe *et al.*, 2004). Although we added AMPPNP for crystallization, we could not observe any electron density for the γ-phosphate. Thus, we placed ADP in the model instead of AMPPNP. The γ-phosphate may be disordered or removed. The adenine nucleotide interacts with Glu67, Lys83, Glu85 and Asp109 in the A1 domain, and Asp485, Gly522 and Asn523 in the A2 domain (Fig. 4*b*). An ADP was found in *Tm*PurL in the monomeric form (PDB entry 2hru) and its interacting residues are Glu51, Lys68, Glu70, Asp94, Asn442, Gly477 and Asn478 (Morar *et al.*, 2006). These amino-acid residues interact with ADP in a similar manner except for Glu67 in *Tt*PurL and Glu51 in *Tm*PurL: Glu67 uses the backbone and Glu51 uses the side chain. The corresponding

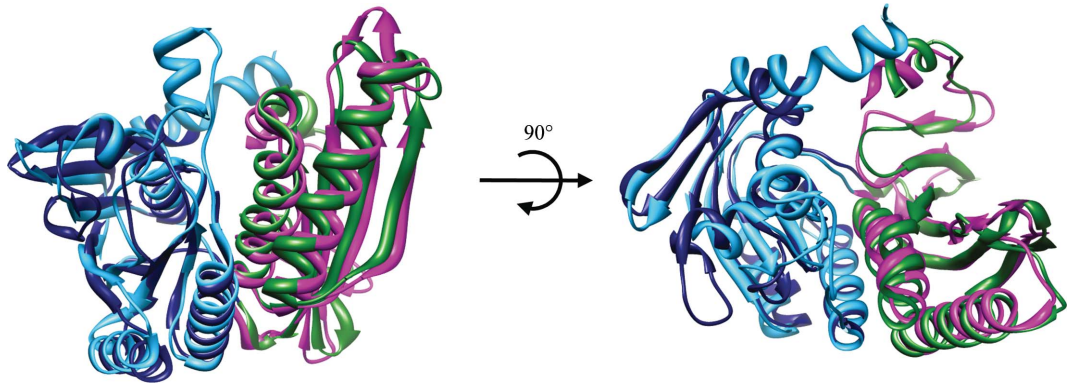

Figure 3
Superposition of the A1–B1 and A2–B2 domains of *Tt*PurL. The same colour scheme is used as in Fig. 1.

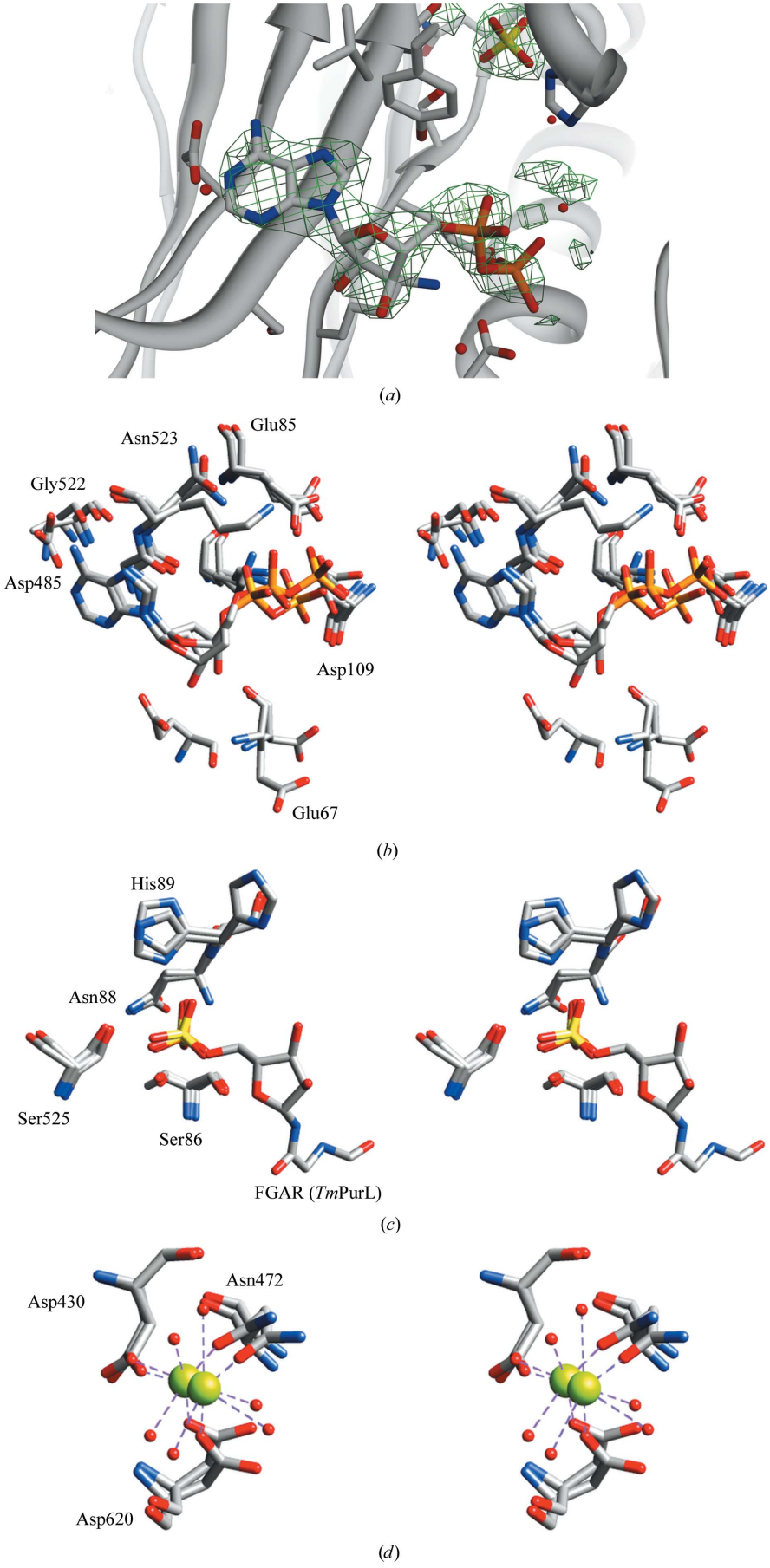

residues in *St*PurL are Asp258, Lys292, Glu294 and Asp318 in the A1 domain, and Ala738, Gly775 and Lys776 in the A2 domain (Anand, Hoskins, Stubbe *et al.*, 2004). The conformation of the loop between $\alpha4$ and $\beta1$ containing the Glu residue varies in *Tt*PurL and *Tm*PurL. The loop in *Tm*PurL is in the open form without adenine nucleotides or with ATP in the active site and in the closed form with ADP or AMPPCP in the active site (Morar *et al.*, 2006). The loop in *Tt*PurL with the adenine nucleotide in the active site is in the closed form. The loop in *St*PurL is in the closed form without adenine nucleotide in the active site, probably because of the inserted sequence which elongates the sheet consisting of $\beta1$ and $\beta2$.

In the case of large PurL (*St*PurL) and the ternary complex (*Tm*PurL, *Tm*PurQ and *Tm*PurS), another adenine nucleotide was found at the *B*-domain side of the A1 and A2 domains, which is thought to be the auxiliary site, indicating that the adenine nucleotide in the auxiliary site is required for complex formation (Morar *et al.*, 2006, 2008). No adenine nucleotides are bound to the auxiliary site of *Tt*PurL without PurQ and PurS, as is the case for *Tm*PurL.

A PO_4^{3-} ion was found at the B1-domain side of the A1 and A2 domains (Fig. 1*a*). It is probable that the PO_4^{3-} ion bound to the protein during purification. The position of PO_4^{3-} in *Tt*PurL corresponds to the position of the 5′-phosphate group of FGAR as bound to *Tm*PurL (PDB entry 2hs3; Morar *et al.*, 2006; Fig. 4*c*). The PO_4^{3-} ion interacts with residues Ser86, Asn88 and His89 in the A1 domain and Ser525 in the A2 domain; the corresponding residues in *Tm*PurL are Ser71, Asn73, His74 and Ser480. A PO_4^{3-} ion was also found in the same position in *St*PurL and the corresponding residues are

Figure 4
Ligands bound to *Tt*PurL. (*a*) The OMIT electron-density map contoured at the 1.0σ level for bound ADP and PO_4^{3-}. (*b*) Bound ADP in *Tt*PurL, *Tm*PurL (PDB entry 2hru) and *St*PurL (PDB entry 1t3t). The C^{α}, C and N atoms in the backbone of Lys83, Glu85, Asp109, Asp485, Gly522 and Asn523 and the corresponding residues in *Tm*PurL and *St*PurL are superimposed. Glu67 and the corresponding residues are shown but not used for superposition. Lys83 is located on the opposite side of the phosphate group of ADP and its label is not shown. (*c*) Bound PO_4^{3-} in *Tt*PurL and *St*PurL (1t3t) and bound FGAR in *Tm*PurL (PDB entry 2hs3). The C^{α}, C and N atoms in the backbone of Ser86, Asn88, His89 and Ser525 and the corresponding residues in *Tm*PurL and *St*PurL are superimposed. (*d*) Bound Mg^{2+} in *Tt*PurL and *St*PurL (PDB entry 1t3t). The C^{α}, C and N atoms in the backbone of Asp430, Asn472 and Asp620 and the corresponding residues in *St*PurL are superimposed.

Thr295, Asp297, His298 and Ser778 (Anand, Hoskins, Stubbe *et al.*, 2004). Thus, these residues form a phosphate-binding site in each PurL. As in *Tt*PurL and *St*PurL, a loop between β7 and α11 is disordered in the absence of FGAR. In *Tm*PurL, helix α10, which recognizes the ribose group of FAGR, is formed upon binding of FGAR (Morar *et al.*, 2006).

A magnesium ion was found in the auxiliary site and its interacting residues are Asp430, Asn472 and Asp620 (Fig. 4*d*). We did not add Mg^{2+} during purification and crystallization. It is probable that the Mg^{2+} ion came from the *E. coli* cell. A corresponding Mg^{2+} ion was found in *St*PurL and the interacting residues are Asp679, Asn722 and Asp884 (Anand, Hoskins, Stubbe *et al.*, 2004). In *St*PurL this Mg^{2+} ion binds to the β-phosphate of bound ADP in the auxiliary site. Thus, Mg^{2+} may support ADP binding to the auxiliary site. In contrast, these residues are not conserved in *Tm*PurL and a corresponding Mg^{2+} was not found even in the ternary complex of *Tm*PurL, *Tm*PurQ and *Tm*PurS (PDB entry 3d54; Morar *et al.*, 2008). It seems that Lys429, which is located at the position corresponding to Asn472 in *Tt*PurL and Asn722 in *St*PurL, is used instead of Mg^{2+}.

3.4. Active-site structure

As described above, the residues interacting with the ligands are well conserved among the three PurLs. In addition, residues in the active site are also conserved: Glu85, Asp109 and Asp259 for γ-phosphate-group binding and His41, His87, Arg108, Gln231 and Gln305 for FGAR binding (Morar *et al.*, 2006). Although the γ-phosphate groups of ATP and FGAR were not found in the crystal structure of *Tt*PurL, the side-chain conformations of these residues are also similar to those in *Tm*PurL and *St*PurL, confirming that structure of the active site is strictly conserved.

During the reaction catalyzed by FGAR amidotransferase, an ammonia molecule is thought to be transferred from the active site of PurQ to that of PurL (Mizobuchi *et al.*, 1968; Anand, Hoskins, Stubbe *et al.*, 2004) and two possible ammonia channels have been proposed for *St*PurL as well as *Tm*PurL (Anand, Hoskins, Stubbe *et al.*, 2004; Morar *et al.*, 2008). As pointed out by Morar and coworkers, one of the two candidates is the more likely path for ammonia (Morar *et al.*, 2008) and the residues forming the channel (Tyr148, Gly233, Ala100, Gln282 and Gly105) are also conserved in *Tt*PurL, together with their side-chain conformation.

In conclusion, a third structure of PurL, *Tt*PurL, has been determined and the structural similarity between *Tt*PurL and *St*PurL, the corresponding domain of the large PurL, has been demonstrated.

We thank Yumiko Inoue, Miwa Ohmori and Maki Uda for protein purification. Molecular-graphics images were produced using the *UCSF Chimera* package from the Resource for Biocomputing, Visualization and Informatics at the University of California, San Francisco (supported by NIH P41 RR001081).

References

Anand, R., Hoskins, A. A., Bennett, E. M., Sintchak, D., Stubbe, J. & Ealick, S. E. (2004). *Biochemistry*, **43**, 10343–10352.
Anand, R., Hoskins, A. A., Stubbe, J. & Ealick, S. E. (2004). *Biochemistry*, **43**, 10328–10342.
Brünger, A. T., Adams, P. D., Clore, G. M., DeLano, W. L., Gros, P., Grosse-Kunstleve, R. W., Jiang, J.-S., Kuszewski, J., Nilges, M., Pannu, N. S., Read, R. J., Rice, L. M., Simonson, T. & Warren, G. L. (1998). *Acta Cryst.* D**54**, 905–921.
Ebbole, D. J. & Zalkin, H. (1987). *J. Biol. Chem.* **262**, 8274–8287.
Hijikata, A., Yura, K., Noguti, T. & Go, M. (2011). *Proteins*, **79**, 1868–1877.
Hoskins, A. A., Anand, R., Ealick, S. E. & Stubbe, J. (2004). *Biochemistry*, **43**, 10314–10327.
Jones, T. A., Zou, J.-Y., Cowan, S. W. & Kjeldgaard, M. (1991). *Acta Cryst.* A**47**, 110–119.
Laskowski, R. A., MacArthur, M. W., Moss, D. S. & Thornton, J. M. (1993). *J. Appl. Cryst.* **26**, 283–291.
Li, C., Kappock, T. J., Stubbe, J., Weaver, T. M. & Ealick, S. E. (1999). *Structure*, **7**, 1155–1166.
Mathews, I. I. *et al.* (2006). *Proteins*, **63**, 1106–1111.
Melnick, I. & Buchanan, J. M. (1957). *J. Biol. Chem.* **225**, 157–162.
Mizobuchi, K., Kenyon, G. L. & Buchanan, J. M. (1968). *J. Biol. Chem.* **243**, 4863–4877.
Morar, M., Anand, R., Hoskins, A. A., Stubbe, J. & Ealick, S. E. (2006). *Biochemistry*, **45**, 14880–14895.
Morar, M., Hoskins, A. A., Stubbe, J. & Ealick, S. E. (2008). *Biochemistry*, **47**, 7816–7830.
Morris, R. J., Perrakis, A. & Lamzin, V. S. (2002). *Acta Cryst.* D**58**, 968–975.
Otwinowski, Z. & Minor, W. (1997). *Methods Enzymol.* **276**, 307–326.
Pettersen, E. F., Goddard, T. D., Huang, C. C., Couch, G. S., Greenblatt, D. M., Meng, E. C. & Ferrin, T. E. (2004). *J. Comput. Chem.* **25**, 1605–1612.
Saxild, H. H. & Nygaard, P. (2000). *Microbiology*, **146**, 807–814.
Terwilliger, T. C. (2000). *Acta Cryst.* D**56**, 965–972.
Terwilliger, T. C. (2003). *Acta Cryst.* D**59**, 38–44.
Terwilliger, T. C. & Berendzen, J. (1999). *Acta Cryst.* D**55**, 849–861.
Ueno, G., Kanda, H., Hirose, R., Ida, K., Kumasaka, T. & Yamamoto, M. (2006). *J. Struct. Funct. Genomics*, **7**, 15–22.
Zhang, Y., Morar, M. & Ealick, S. E. (2008). *Cell. Mol. Life Sci.* **65**, 3699–3724.